Evidence for a Functional Role of the Dynamics of Glycine-121 of *Escherichia coli* Dihydrofolate Reductase Obtained from Kinetic Analysis of a Site-Directed Mutant†

Craig E. Cameron‡ and Stephen J. Benkovic*

Department of Chemistry, The Pennsylvania State University, University Park, Pennsylvania 16802

Received July 7, 1997; Revised Manuscript Received October 14, 1997⊗

ABSTRACT: Two-dimensional heteronuclear ($^1H-^{15}N$) nuclear magnetic relaxation studies of dihydrofolate reductase (DHFR) from *Escherichia coli* have demonstrated that glycine-121 which is 19 Å from the catalytic center of the enzyme has large-amplitude backbone motions on the nanosecond time scale [Epstein, D. M., Benkovic, S. J., and Wright, P. E. (1995) *Biochemistry 34*, 11037−11048]. In order to probe the dynamic−function relationships of this residue, we constructed a mutant enzyme in which this glycine was changed to valine. Equilibrium binding studies indicated that the Val-121 mutant retained wild-type binding properties with respect to dihydrofolate and tetrahydrofolate; however, binding to NADPH and $NADP^+$ was decreased by 40-fold and 2-fold, respectively, relative to wild-type DHFR. Single-turnover experiments indicated that hydride transfer was reduced by 200-fold to a rate of 1.3 s^{-1} and was the rate-limiting step in the steady state. Interestingly, pre-steady-state kinetic analysis of the Val-121 mutant revealed a conformational change which preceded chemistry that occurred at a rate of 3.5 s^{-1}. If this step exists in the kinetic mechanism of the wild-type enzyme, then it would be predicted to occur at a rate of approximately 2000 s^{-1}. Glycine-121 was also changed to alanine, serine, leucine, and proline. While the Ala-121 and Ser-121 mutants behaved similar to wild-type DHFR, the Leu-121 and Pro-121 mutants behaved like Val-121 DHFR in that hydride transfer was the rate-limiting step in the steady state and a conformational change preceding chemistry was observed. Finally, insertion of a glycine or valine between amino acids 121 and 122 produced mutant enzymes with properties similar to wild-type or Val-121 DHFRs, respectively. Taken together, these results provide compelling evidence for dynamic coupling of a remote residue to kinetic events at the active site of DHFR.

Dihydrofolate reductase (5,6,7,8-tetrahydrofolate:$NADP^+$ oxidoreductase, EC 1.5.1.3; DHFR)[1] catalyzes the NADPH-dependent reduction of 7,8-dihydrofolate (H_2F) to 5,6,7,8-tetrahydrofolate (H_4F). Tetrahydrofolate-based cofactors are a source of single-carbon units in various oxidation states required for biosynthesis of biomolecules, such as nucleotides and amino acids. The essential role of this enzyme in a variety of anabolic pathways makes this enzyme an outstanding target for the development of antiproliferative therapeutics. In fact, the most commonly used drug in the treatment of cancer is methotrexate (MTX), which is a tight-binding inhibitor of DHFR. As a result of the biological and pharmacological importance of DHFR, this enzyme has been the subject of intensive structural and kinetic investigation for many years. Structural models based on X-ray crystallographic data have been constructed for *Escherichia coli* DHFR in the absence and presence of a variety of substrates, inhibitors, and cofactors (*1* and references cited therein). Also, information on the dynamics of this enzyme based on NMR data exists (*2*, *3*). Moreover, a complete kinetic scheme capable of predicting the behavior of this enzyme under a variety of conditions has been described (*4*).

As a result of the wealth of information available for *E. coli* DHFR, this enzyme represents an ideal system to investigate the molecular basis of enzymic catalysis. For example, while it is clear that enzymes have molecular motions on various time scales (*5*, *6*), an essential and direct role for these conformational fluctuations in catalysis has yet to be established. Falzone *et al.* have used two-dimensional NMR to correlate the dynamics of a flexible loop in *E. coli* DHFR that occur on the millisecond time scale with steady-state turnover of this enzyme (*2*). In addition, Farnum *et al.* have used fluorescence lifetime measurements to correlate molecular motions that occur on the nanosecond time scale with the rate of DHFR-catalyzed hydride transfer (*7*).

Recently, Epstein *et al.* have used two-dimensional, heteronuclear ($^1H-^{15}N$) nuclear magnetic relaxation methods to study the backbone dynamics of *E. coli* DHFR complexed with folate (*3*) . These studies provided dynamic information on this enzyme−substrate complex over a time scale ranging from picoseconds to milliseconds. Succinctly, these investigators found conformational fluctuations on the nanosecond time scale to be restricted to *E. coli* DHFR loop 1, the βF−βG loop (in particular, residue 121), and the hinge between the adenosine-binding domain and the major domain. Interestingly, mutational and kinetic analyses have implicated loop 1 in transition state stabilization (*8*), and X-ray crystallographic data have implicated the latter two structural

† This work was supported in part by NIH Grant GM24129.

* To whom correspondence should be addressed. Telephone: 814-865-2882. Fax: 814-865-2973. E-Mail: sjb1@psu.edu.

‡ Recipient of a NIH Postdoctoral Fellowship (AI09076).

⊗ Abstract published in *Advance ACS Abstracts,* December 1, 1997.

[1] Abbreviations: DHFR, dihydrofolate reductase; Val-121 DHFR, *E. coli* DHFR mutant in which glycine-121 is changed to valine; H_2F, 7,8-dihydrofolate; H_4F, 5,6,7,8-tetrahydrofolate; MTX, methotrexate; NADPH, nicotinamide adenine dinucleotide phosphate reduced; NADPD, [(4′*R*)-^{2}H]NADPH; DNADPH, 5,6-dihydroNADPH; $NADP^+$, nicotinamide adenine dinucleotide phosphate oxidized; EDTA, ethylenediaminetetraacetic acid; DTT, dithiothreitol.

S0006-2960(97)01623-1 CCC: $14.00

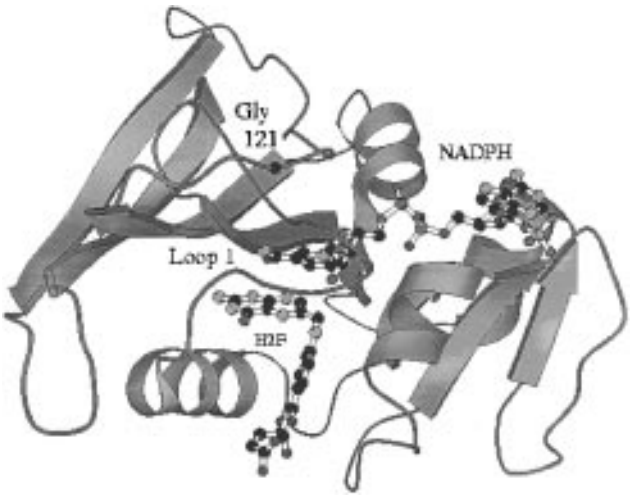

FIGURE 1: Structural model for *E. coli* DHFR complexed with H_2F and NADPH. The position of glycine-121 in the βF−βG loop is indicated relative to loop 1. The graphics were constructed with Molscript (*10*).

elements in ligand-dependent conformational changes (*9*). The authors therefore hypothesized that the observed time-dependent, structural fluctuations may be related to the catalytic properties of the enzyme.

The βF−βG loop (residues 117−131) is 19 Å from the catalytic center of *E. coli* DHFR (Figure 1) (*9*). However, upon binding of folate, this loop collapses inward toward loop 1 (*9*). Based on the crystallographic *B*-factors for residues 117−131, this loop is quite flexible (*9*). Gly-121, which is strictly conserved in all prokaryotic DHFRs, is at the center of this loop. This residue is flanked by Glu-120 and Asp-122, both of which are disordered (*9*), and is adjacent to a β-bulge consisting of Asp-122 and Thr-123. Gekko *et al.* have shown that changing this conserved glycine to valine or leucine decreased the steady-state rate of hydride transfer at pH 7.0 approximately 20-fold relative to the wild-type enzyme without affecting the K_m for H_2F (*11*). However, only modest changes were observed in the CD spectra and the thermodynamic parameters for urea and thermal denaturation, suggesting that these mutations did not produce global alterations in the structure or stability of these enzymes (*11*).

Taken together, the observations of Epstein *et al.* and Gekko *et al.* could be interpreted to mean that the conformational fluctuations of the βF−βG loop are important for efficient release of product since the steady-state rate of hydride transfer at pH 7.0 for wild-type DHFR corresponds to dissociation of H_4F from the DHFR−H_4F−NADPH complex (*4*). Unfortunately, based on the studies of Gekko and colleagues alone, this conclusion may not be valid because this study did not provide data to demonstrate directly that the rate measured in the steady state for the Val-121 and Leu-121 mutants reflects the same step measured in the steady state for wild-type DHFR.

In this study, we have constructed a partial kinetic scheme for the Val-121 mutant of *E. coli* DHFR at pH 7.0. While this mutant enzyme binds H_2F and H_4F as efficiently as wild-type DHFR, binding to NADPH and $NADP^+$ was decreased by 40-fold and 2-fold, respectively. Furthermore, in contrast to what is observed for the wild-type enzyme, hydride transfer limited steady-state turnover of the Val-121 mutant. The observed change in the rate of hydride transfer reflects a 200-fold decrease relative to wild-type DHFR. Moreover, changing the conserved glycine-121 to valine revealed a conformational change that precedes the chemical step in the kinetic mechanism of DHFR. In addition, it appears that only serine or alanine substitutions at position 121 can be made without altering the kinetic scheme for DHFR-catalyzed hydride transfer. It must be noted, however, that these enzymes are still compromised in terms of catalytic efficiency relative to that of wild-type DHFR. These results provide compelling evidence for dynamic coupling of a remote residue to kinetic events at the active site of DHFR.

MATERIALS AND METHODS

Substrates. 7,8-Dihydrofolate (H_2F) was prepared by dithionite reduction as described by Blakely (*12*). (6*S*)-5,6,7,8-Tetrahydrofolate (H_4F) was prepared from H_2F by enzymatic conversion using wild-type dihydrofolate reductase (DHFR) as described by Mathews and Huennekens (*13*). H_4F was purified by DE-52 chromatography as described by Curthoys *et al.* (*14*). [(4′*R*)-^{2}H]NADPH (NADPD) was prepared by reduction of $NADP^+$ using an $NADP^+$-dependent alcohol dehydrogenase (EC 1.1.1.2) from *Thermoanaerobium brockii* (obtained from Sigma) and 2-propanol-d_8 (obtained from Aldrich) and purified by reverse-phase HPLC as described by Jeong and Gready (*15*). 5,6-Dihydronicotinamide adenine dinucleotide phosphate reduced (DNADPH) was a gift of Dr. Hyeung-geun Park (The Pennsylvania State University). NADPH, $NADP^+$, MTX, and folate were purchased from Sigma. The following extinction coefficients were used: H_4F, 28 000 M^{-1} at 397 nm, pH 7.5 (*16*); H_2F, 28 000 M^{-1} at 282 nm, pH 7.4 (*17*); MTX, 22 100 M^{-1} at 302 nm in 0.1 N KOH (*18*); NADPH, 6200 M^{-1} at 339 nm, pH 7.0 (*19*); $NADP^+$, 18 000 M^{-1} at 259 nm, pH 7.0 (*19*); DNADPH, 18 000 M^{-1} at 259 nm, pH 7.0 [Hyeung-geun Park, personal communication].

Biochemicals. All reagents were molecular biology grade from Sigma. All ion-exchange and affinity resins were from Sigma. All enzymes required for recombinant DNA methods were obtained from New England Biolabs.

Buffers. MTEN: 50 mM 2-morpholinoethanesulfonic acid, 25 mM Tris, 25 mM ethanolamine, and 100 mM NaCl, pH 7.0. Buffer A: 25 mM sodium phosphate, pH 7.0, 10% glycerol, and 5 mM EDTA. Buffer B: 25 mM sodium phosphate, pH 7.0, 10% glycerol, 0.5 M NaCl, and 18% polyethyleneglycol-8000. Buffer C: 25 mM sodium phosphate, pH 7.0, 10% glycerol, 0.5 M NaCl, and 1 mM DTT. Buffer D: 100 mM sodium borate, 10% glycerol, 0.5 M NaCl, 3 mM folic acid, and 1 mM DTT at pH 9.5. Buffer E: 50 mM Tris, pH 7.5, 10% glycerol, and 1 mM DTT.

Construction of Expression Vectors. A synthetic gene coding for *E. coli* DHFR was amplified from the plasmid pTZwt1-3 (*8*) using standard PCR methods (*20*). The forward primer introduced a unique *Nde*I restriction site, and the reverse primer introduced a unique *Bam*HI restriction site. The sequence of the forward primer (DHFR-for) is 5′-GCG GGA TCC CAT ATG ATC AGT CTG ATT GCG GCG-3′. The sequence of the reverse primer (DHFR-rev) is 5′-GCG TCT AGA GGA TCC TTA ACG ACG CTC GAG GAT-3′. The PCR product was purified by gel (*21*) and digested with *Nde*I and *Bam*HI. The cut fragment was ligated into pET22b (Novagen) which had been digested with the same restriction enzymes. Overlap−extension PCR

methods (*22*) were used to construct Val-121 DHFR. The sequence of the mutagenic, forward primer (V121-for) is 5′-C GAT GCA GAA GTC GAA GTC GAC ACC CAT TTT-3′. The site of the mutation is underlined. The sequence of the mutagenic, reverse primer (V121-rev) is 3′-TA CGT CTT CAG CTT CAG CTT CAG CTG TGG GTA AAA GGC C-5′. Briefy, two separate PCR reactions were completed: one reaction with DHFR-for and V121-rev; the other with V121-for and DHFR-rev. Both reactions used pET22b-DHFR as the template. The resulting products were purified by gel and used as the template for a PCR reaction using DHFR-for and DHFR-rev as the sole primers. The resulting product was purified, digested with *Cla*I and *Bam*HI, and ligated into pET22b-DHFR which had been digested with the same restriction enzymes. Glycine-121 was also changed individually to leucine and proline. These mutant enzymes were constructed as described above using mutagenic primers in which the underlined codon in the forward primer was changed to CTC or CCC to encode leucine or proline, respectively. Construction of an additional 121 mutants took advantage of the nearby *Cla*I site. PCR primers were synthesized which contained the *Cla*I site and appropriate mutation. PCR was completed using the *Cla*I-containing, mutant primer in combination with the DHFR-rev primer. The purified product was digested with *Cla*I and *Eco*RI and ligated into pET22b-DHFR which had been digested with these enzymes. The oligonucleotide sequences are as follows: (1) 5′-ACG CAT **ATC GAT** GCA GAA GTG GAA GCC GAC ACC CAT TTT CCG G-3′, which changes Gly-121 to Ala; (2) 5′-ACG CAT **ATC GAT** GCA GAA GTG GAA AGT GAC ACC CAT TTT CCG G-3′, which changes Gly-121 to Ser; (3) 5′-ACG CAT **ATC GAT** GCA GAA GTG GAA GGC GGC GAC ACC CAT TTT CCG G-3′, which inserts a Gly between Gly-121 and Asp-122; (4) 5′-ACG CAT **ATC GAT** GCA GAA GTG GAA GGC GTG GAC ACC CAT TTT CCG G-3′, which inserts a Val between Gly-121 and Asp-122. Constructs were verified by automated DNA sequencing by the Penn State Nucleic Acid Facility. Oligonucleotide were synthesized on an Expedite 8909 DNA/RNA synthesizer (PerSeptive Biosystems) following the manufacturer's protocol.

Expression and Purification of Wild-Type and Mutant DHFRs. The *E. coli* strain BL21(DE3) was used for expression. Cells were grown at 37 °C in NZCYM media (Gibco-BRL) containing 200 μg/mL ampicillin to an OD_{600} of 0.8. Isopropyl β-D-thiogalactoside was added to a final concentration of 0.4 mM, and the cells were grown an additional 4−5 h. Cells were harvested by centrifugation (3000*g* for 10 min). Cells (5 g) were suspended in 25 mL of buffer A and lysed by lysozyme (1 mg/mL). The lysate was brought to 0.5 M NaCl followed by the slow addition of 23 mL of buffer B. The lysate was then clarified by centrifugation (50000*g* for 35 min). This extract was loaded onto a 5 mL MTX−agarose column which had been preequilibrated with 500 mL of buffer C. After the extract was loaded, the column was washed with 50 mL of buffer C and eluted with 10−15 mL of buffer D. Fractions (1.0 mL) were collected manually, and the protein concentration of each was measured using the Bio-Rad protein assay. Peak fractions (usually fractions 2−8) were pooled and dialyzed from 2 h to overnight against 1 L of buffer E. The dialyzed protein was loaded onto a 15 mL DE-52 (Whatman) column which had been preequilibrated with 150 mL of buffer E. After loading, the column was washed with 50 mL of buffer E and then eluted with a 40 mL × 40 mL gradient of 0−0.5 M NaCl in buffer E. Peak fractions were pooled and dialyzed against buffer A followed by concentration. Protein concentration was determined by fluorescence titration with MTX.

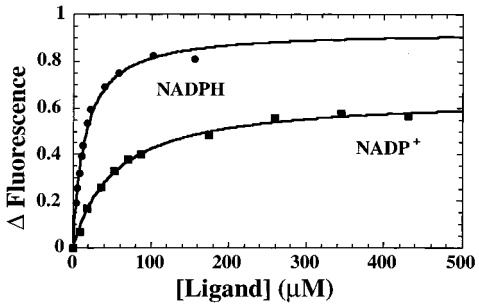

FIGURE 2: Measurement of the K_d for NADPH (●) and $NADP^+$ (■) binding to Val-121 DHFR by monitoring the quenching of intrinsic fluorescence. Fluorescence titrations were completed using 0.1 μM Val-121 DHFR and the indicated concentrations of ligand. The solid lines represent the fit of the data to a hyperbola.

Thermodynamic Dissociation Constants. The thermodynamic binding of ligands (K_d) was measured by following the quenching of instrinsic enzyme fluorescence at 340 nm upon excitation at 290 nm as a function of added ligand on an SLM 8000 spectrofluorometer. Control experiments were performed in which a known quantitiy of tryptophan was titrated to correct for inner filter absorbance effects. Typically, the enzyme concentration was less than the K_d of the ligand.

Kinetics of Binding and Pre-Steady-State Kinetics. Transient binding and pre-steady-state kinetic experiments were performed on a Applied Photophysics stopped-flow spectrophotometer. Ligand binding and competition were measured by following the quenching of intrinsic enzyme fluorescence as described previously (*4*). The sample was excited at 290 nm and the emission measured using a 250−400 nm output filter. Hydride transfer was measured by following fluorescence energy transfer from the protein to the reduced nicotinamide moiety of NADPH as described previously (*4*). The sample was excited at 290 nm and the emission measured using a 400 nm output filter. Absorbance measurements were performed at 340 nm. Typically 4−8 traces were recorded and averaged for data analysis. The data were fit by nonlinear least-squares methods as indicated in the various figure legends using the program KaleidaGraph (Abelbeck Software Inc.)

RESULTS

Thermodynamic Binding of Ligands. The thermodynamic dissociation constants (K_d) for binding of NADPH, DNADPH, $NADP^+$, H_2F, and H_4F to the Val-121 mutant were measured by using quenching of intrinsic enzyme fluorescence as described under Materials and Methods. Titrations of the Val-121 mutant with NADPH and $NADP^+$ are shown in Figure 2. The K_d values for all ligands are listed in Table 1 and are compared to wild-type DHFR. The binding affinity of the Val-121 mutant for NADPH decreased 40-fold relative to the wild-type enzyme, and that of $NADP^+$ decreased by only 2-fold. DNADPH binding to the Val-121 mutant and wild-type DHFR was approximately 2-fold stronger for both

Table 1: Equilibrium Binding Constants (μM) for Ligands to Val-121 and Wild-Type DHFRs at 25 °C in MTEN Buffer at pH 7.0

ligand	Val-121	WT
NADPH	14.2 ± 0.8	0.44 ± 0.01
DNADPH	8.3 ± 0.4	0.25 ± 0.02
$NADP^+$	52 ± 3	24 ± 1
H_2F	0.36 ± 0.02	0.25 ± 0.02
H_4F	0.30 ± 0.04	0.16 ± 0.02

Table 2: Dissociation Rate Constants (s^{-1}) for Ligands from Val-121 and Wild-Type DHFRs at 25 °C in MTEN Buffer at pH 7.0

ligand	enzyme species	trap	Val-121	WT[a]
NADPH	E−NADPH	$NADP^+$	248 ± 25	3.6 ± 0.5
	E−H_4F−NADPH		282 ± 13	85 ± 10
DNADPH	E−H_2F−DNADPH	NADPH	462 ± 40	
$NADP^+$	E−$NADP^+$	NADPH	204 ± 11	290 ± 20
	E−H_2F−$NADP^+$		913 ± 210	50 ± 10
	E−H_4F−$NADP^+$		>1000	200 ± 20
H_2F	E−H_2F	MTX	14 ± 1	22 ± 5
	E−DNADPH−H_2F		19 ± 1	43 ± 6
	E−$NADP^+$−H_2F		17 ± 1	7 ± 1
H_4F	E−H_4F	MTX	1.3 ± 0.1	1.4 ± 0.2
	E−NADPH−H_4F		1.9 ± 0.3	12 ± 2
	E−DNADPH−H_4F		1.9 ± 0.1	
	E−$NADP^+$−H_4F		1.9 ± 0.2	2.4 ± 0.2

[a] Taken from Fierke *et al.* (1987).

enzymes when compared to NADPH binding. Binding of H_2F and H_4F to the Val-121 mutant was essentially unchanged.

Kinetic Binding of Ligands. The rate of H_2F and H_4F binding was determined by measuring the time dependence of quenching of the intrinsic enzyme fluorescence after rapid mixing of the enzyme and ligand in a stopped-flow apparatus as described under Materials and Methods. The reactions were pseudo-first-order with respect to the ligands; therefore, $k_{obs} = k_{on}[L] + k_{off}$ where k_{on} and k_{off} are the association and dissociation rate constants, respectively, and [L] is the concentration of ligand analyzed. By plotting k_{obs} as a function of [L], k_{on} can be obtained from the slope and k_{off} from the intercept of the resulting line. The values for k_{on} were 40 ± 4 μM^{-1} s^{-1} and 4 ± 0.5 μM^{-1} s^{-1} for H_2F and H_4F, and for k_{off} were 15 ± 5 s^{-1} and 1 ± 1 s^{-1} for H_2F and H_4F. When compared to the wild-type enzyme, the only significant change observed was for the k_{on} for H_4F which was decreased by a factor of 6.

Attempts to assess the kinetics of binding of NADPH and $NADP^+$ to the Val-121 mutant were unsuccessful. No fluorescence change was observed on the millisecond time scale when the ligand was either NADPH or $NADP^+$. However, a slow, ligand-independent fluorescence change was observed which occurred at a rate of 0.08 ± 0.01 s^{-1}. This ligand-independent transient has been observed for wild-type DHFR and has been attributed to the conversion of DHFR from the E_2 conformer, which binds NADPH weakly, to the E_1 conformer, which binds this ligand tightly (*4*).

Dissociation Rate Constants for Ligands. The dissociation rate constants of all ligands from the various binary and ternary complexes were measured by using a competition method as described previously (*4*) and are listed in Table 2. This method takes advantage of the difference between the fluorescence end points for two ligands. The difference between the end points for NADPH and $NADP^+$ can be seen in Figure 2. The competition experiment is diagrammed in Scheme 1. In this experiment, an enzyme−ligand complex (E−L_1) is formed and then rapidly mixed with a large excess of a competing ligand (L_2). The dissociation of L_1 from the E−L_1 complex produces free E which in turn will be bound by L_2 following an exponential process which occurs at a rate equivalent to k_{off} (k_{-1}) for L_1 when $k_1[L_1] << k_2[L_2] >> k_{-1}$.

Scheme 1

$$\mathbf{E\text{-}L_1} \underset{k_1}{\overset{k_{-1}}{\rightleftharpoons}} \mathbf{E + L_1}$$

$$\mathbf{E + L_2} \underset{k_{-2}}{\overset{k_2}{\rightleftharpoons}} \mathbf{E\text{-}L_2}$$

The competition method was also used to determine the dissociation rate constants for all possible binary and ternary complexes. In order to approximate k_{off} for H_2F and NADPH from the reactive ternary complex, DNADPH was used instead of NADPH. In spite of the fact that DNADPH cannot be used as a cofactor for reduction of H_2F, this molecule binds to wild-type DHFR in a manner very similar to NADPH (Table 1). Because k_{off} for DNADPH and $NADP^+$ from all complexes studied was much faster than hydride transfer, NADPH could be used as a trapping ligand.

Consistent with the equilibrium binding studies, k_{off} for NADPH from E−NADPH was increased by approximately 70-fold relative to wild-type DHFR. However, k_{off} for NADPH from the E−H_4F−NADPH complex was increased by only 3-fold relative to the wild-type enzyme. Surprisingly, the rate of $NADP^+$ release from ternary complexes containing either H_2F or H_4F was increased by at least 5-fold relative to the binary complex. This was not the case for wild-type DHFR. Finally, there was a 6-fold decrease in k_{off} measured for H_4F from the E−H_4F−NADPH complex. The values of the remaining dissociation rate constants were in close agreement with those measured by Fierke *et al.* for the wild-type enzyme (*4*).

Pre-Steady-State Kinetics. Stopped-flow fluorescence and absorbance can be used to measure DHFR-catalyzed hydride transfer. The ability to monitor hydride transfer by stopped-flow fluorescence results from the overlap of the emission maximum of the protein at 340 nm with the excitation maximum of the reduced nicotinamide moiety of NADPH. The emission maximum of NADPH is 450 nm, and the oxidized nicotinamide moiety of $NADP^+$ displays no emission at this wavelength. Therefore, conversion of NADPH to $NADP^+$ results in a decrease in the relative fluorescence intensity. Moreover, since the fluorescence resonance energy transfer process between the protein and NADPH is dependent on distance and environment (*23*), protein or coenzyme conformational changes that alter either of these properties can be monitored. The ability to use stopped-flow absorbance to monitor hydride transfer results from the large difference in molar extinction coefficients for NADPH relative to $NADP^+$ at 340 nm.

Single Turnover Experiment. Stopped-flow fluorescence was used to measure hydride transfer under conditions of excess enzyme. Using these conditions, the rate of the step which limits conversion of H_2F to H_4F is measured. In the

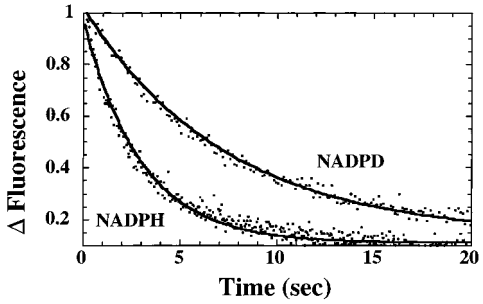

FIGURE 3: Measurement of the rate of hydride transfer catalyzed by Val-121 DHFR in a single turnover measured by stopped-flow fluorescence energy transfer. Val-121 DHFR was preincubated with NADPH or NADPD, and the reaction was initiated by addition of H_2F. Final conditions were enzyme (20 μM), cofactor (2 μM), and substrate (100 μM). Solid lines represent the fit of the data to a single exponential decay.

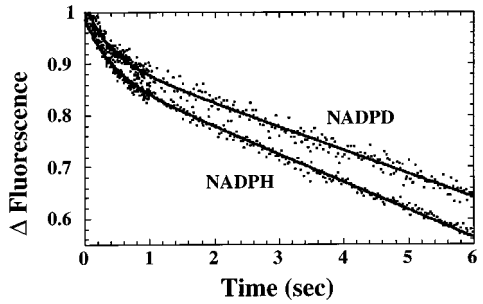

FIGURE 4: Measurement of a pre-steady-state burst for Val-121 DHFR by stopped-flow fluorescence energy transfer. Val-121 DHFR was preincubated with NADPH or NADPD, and the reaction was initiated by addition of H_2F. Final conditions were enzyme (2 μM), cofactor (150 μM), and substrate (100 μM). Solid lines represent the fit of the data to a single exponential decay followed by a linear steady-state rate.

experiment shown in Figure 3, 40 μM Val-121 DHFR was preincubated with 4 μM NADPH and rapidly mixed with 200 μM H_2F (note that the mixing process results in a 2-fold dilution). The change in fluorescence as a function of time was fit to a single exponential and occurred at a rate of 0.34 s^{-1}. When this experiment was repeated using 4 μM NADPD, the observed rate was 0.14 s^{-1} (Figure 3). This corresponds to a primary isotope effect of 2.4. When 40 μM Val-121 DHFR was preincubated with 4 μM H_2F and rapidly mixed with 300 μM NADPH, the observed rate of hydride transfer was 1.3 s^{-1} (data not shown). The difference in reaction rates observed by changing the order of addition is caused by the 10-fold increase in the dissociation rate constants for NADH from both the binary and ternary complexes relative to that of H_2F. The magnitudes of these changes have been confirmed by kinetic simulations (data not shown).

Multiple Turnover Experiments. Hydride transfer catalyzed by Val-121 DHFR was also measured by stopped-flow fluorescence under conditions of excess substrate and cofactor. Val-121 DHFR was preincubated with 300 μM NADPH and rapidly mixed with 200 μM H_2F. The resulting time course is shown in Figure 4. These data were fit to a single exponential decay followed by a linear phase. An apparent burst of product formation occurred at a rate of 3.5 s^{-1}. When this experiment was completed using 300 μM NADPD (Figure 4), the rate of the exponential phase was 3.5 s^{-1}; however, a 2-fold decrease in the amplitude was noted. An isotope effect of 2.1 was observed on the

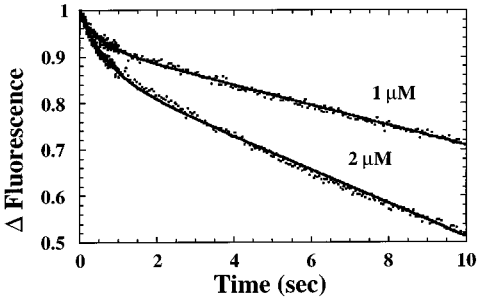

FIGURE 5: Measurement of the dependence of the pre-steady-state burst on the concentration of Val-121 DHFR. This experiment was completed as described in the legend to Figure 3. Final enzyme concentrations were either 1 or 2 μM. Solid lines represent the fit of the data to a single exponential decay followed by a linear steady-state rate.

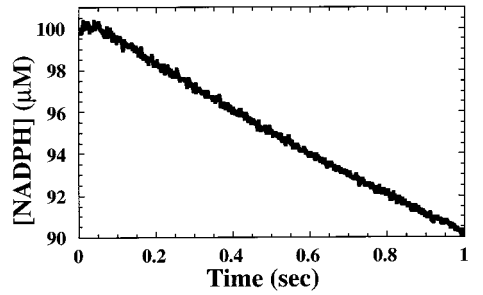

FIGURE 6: Time course for hydride transfer catalyzed by Val-121 DHFR measured by stopped-flow absorbance. This experiment was completed as described in the legend to Figure 3.

slope of the linear phase. In order to determine if the rate of the exponential phase was dependent on enzyme concentration, an experiment was completed as described above with either 1 μM or 2 μM Val-121 DHFR (after mixing). The resulting time courses are shown in Figure 5. Again, the rate of the exponential phase was 3.5 s^{-1}, and the amplitude of this exponential doubled as expected. In order to determine if the exponential phase observed using fluorescence was indeed the result of product formation, an experiment was completed using stopped-flow absorbance. Twenty micromolar Val-121 was preincubated with 200 μM NADPH and rapidly mixed with 200 μM H_2F. The time course for this experiment is shown in Figure 6. A 50 ms lag in product formation is observed prior to the consumption of NADPH at a rate of approximately 1 s^{-1}. The absence of a burst phase in the absorbance mode argues for its presence in the fluorescence mode arising from a conformational change in the active site and/or cofactor.

Reverse Reaction. In order to investigate the kinetics of the reverse reaction, an experiment was completed in which 50 μM H_4F and 500 μM $NADP^+$ were incubated with either 10 μM or 20 μM Val-121 DHFR. The progress of these reactions was monitored by measuring the change in absorbance at 340 nm. These time courses were fit to a linear rate of 0.01 s^{-1} (data not shown).

Additional Mutational Analysis of the βF−βG Loop. (A) Substitutions at 121. The observation that changing glycine-121 to valine produces a mutant DHFR with substantially altered kinetic properties relative to the wild-type enzyme prompted the construction and evaluation of additional amino acid substitutions at this position. Mutant enzymes in which glycine-121 was changed to alanine, serine, leucine, or proline were constructed and purified as described under Materials and Methods. Pre-steady-state kinetic analysis of

Table 3: Rate Constants (s^{-1}) for the Conformational Change and Hydride Transfer for Wild-Type and Mutant DHFRs at 25 °C in MTEN Buffer at pH 7.0

enzyme	k_{conf}[a]	k_{hyd}[b]
Gly-121 (wild-type)	nd[c]	220
Val-121	3.5	1.4
Leu-121	1.0	0.2
Pro-121	3.7	0.5
Ala-121	nd	38.5
Ser-121	nd	40.1
Gly-121+Gly[d]	nd	57
Gly-121+Val[e]	2.0	0.7

[a] Rate constant for the conformational change preceding hydride transfer. [b] Rate constant for hydride transfer. [c] Not detectable. [d] Mutant DHFR containing an insertion of glycine between amino acids 121 and 122. [e] Mutant DHFR containing an insertion of valine between amino acids 121 and 122.

theses mutant enzymes was performed, and the results are shown in Table 3. Changing glycine-121 to leucine or proline produced enzymes with kinetic properties similar to Val-121 DHFR—that is, a fluorescence transient preceding hydride transfer was apparent for both enzymes that occurred at rates of 1.0 and 3.7 s^{-1}, respectively. This fluorescence transient was again attributed to a conformational change. Also, both the leucine and proline substitutions produced enzymes in which hydride transfer was rate-limiting in the steady state and occurred at a rate of 0.2 and 0.5 s^{-1}, respectively. Interestingly, changing glycine-121 to alanine or serine produced enzymes with kinetic properties similar to wild-type DHFR—that is, a conformational change preceding hydride transfer was not detectable for either of these mutants. However, the rate of hydride transfer was, in fact, decreased to 38.5 and 40.1 s^{-1} for the Ala-121 and Ser-121 DHFRs. respectively.

(B) Insertions at 121. Because all of the substitutions at position 121 resulted in DHFRs with reduced rates of hydride transfer, it is quite clear that the glycine at this position is critical for the high catalytic efficiency observed with *E. coli* DHFR. However, the aforementioned mutational analysis does not address whether it is the absence of the amino acid side chain which is important or the ability of glycine to permit this region of the βF−βG loop to adopt a conformation which is important. We reasoned that if the latter possibility was the cause of the changes in the kinetic properties of the mutant enzymes, then insertion of amino acid residues after 121 might be as deleterious as amino acid substitutions at 121. Mutant DHFRs with insertions of either glycine (Gly-121+Gly) or a valine (Gly-121+Val) were constructed and purified as described under Materials and Methods. Pre-steady-state kinetic analysis of these mutants demonstrated that the insertion of a glycine produces an enzyme with kinetic properties similar to wild-type DHFR (Table 3) and insertion of a valine produces an enzyme with kinetic properties similar to Val-121 DHFR. It should be noted that the insertion of glycine between amino acids 121 and 122 caused a 4-fold decrease in the rate of hydride transfer (Table 3).

DISCUSSION

An understanding of the molecular basis for enzymic catalysis is the primary goal of mechanistic enzymology. The wealth of information available for *E. coli* DHFR, including structural (*1*), dynamic (*2*, *3*), kinetic (*4*), and computational (*24*) information, makes this system well-suited for the experimental investigation and verification of the properties of enzymes required for catalysis. All proteins exhibit dynamic features on a variety of time scales ranging from picoseconds to milliseconds (*5*, *6*). The significance of these dynamic properties of proteins to function, however, has been the subject of much discussion (*1*, *2*, *3*, *25*, and references cited therein). It is possible that conformational fluctuations of enzymes contribute to their catalytic properties. In the case of DHFR, this possibility is supported by indirect correlations between rates of hydride transfer and fluorescence lifetime measurements which are presumably a direct reflection of enzyme dynamics (*7*).

Recently, Epstein, Benkovic, and Wright (*3*) used heteronuclear ($^1H-^{15}N$) nuclear magnetic relaxation methods to investigate the backbone dynamics of an *E. coli* DHFR−folate complex. This study showed that conformational fluctuations of this complex with the largest amplitudes on the nanosecond time scale were restricted to regions of the protein implicated in either transition-state stabilization or ligand-dependent conformational changes. Of particular interest to us was Gly-121. This residue is at the center of the βF−βG loop of this enzyme and is 19 Å from the catalytic center (Figure 1). Crystallographic studies implicated this loop in ligand-dependent conformational changes (*9*). Moreover, mutational analysis of this residue demonstrated a 20-fold decrease in the steady-state rate relative to wild-type DHFR when this residue was changed to valine or leucine (*11*). Taken together, it seemed likely that the function of Gly-121 might be related to the dynamic properties of this residue.

To test this hypothesis, we have constructed, purified, and characterized an *E. coli* DHFR mutant in which the glycine at position 121 was changed to a valine. Equilibrium binding studies showed that the only significant difference in ligand binding between the mutant and wild-type DHFRs was a 40-fold increase in the K_d for NADPH (Table 1). This observed increase in the K_d was primarily the result of an increase in the k_{off} for this ligand (Table 2). Interestingly, when the kinetics of NADPH binding were studied by stopped-flow fluorescence, only a slow fluorescence transient was observed, and this change was independent of the concentration of NADPH (data not shown).

There is no definitive explanation, at this time, for the effects of the G121V substitution being restricted to NADPH binding, with the most pronounced effect being observed with free enzyme. However, it is worth noting that there is a substantial difference observed in the stability of a complex comprised of wild-type DHFR and NADPH relative to one comprised of wild-type DHFR and $NADP^+$. Furthermore, in spite of the wealth of structural information available for DHFR and various binary and ternary complexes, the molecular basis for this difference remains obscure. A recent report by Sawaya and Kraut (1) suggests that three conformational states of DHFR exist: open, closed, and occluded, and different DHFR complexes appear to prefer different conformations. Therefore, it is plausible that the conformation preferred by NADPH for binding to DHFR is different than that preferred by $NADP^+$, and the G121V substitution affects one conformation more than the other. A similar argument could also be developed to explain the minimal effect of NADPH binding to the DHFR−H_4F complex and changes in the observed rates of hydride transfer caused by

Scheme 2: Kinetic Scheme for Val-121 Dihydrofolate Reductase at 25 °C in MTEN Buffer at pH 7.0[a]

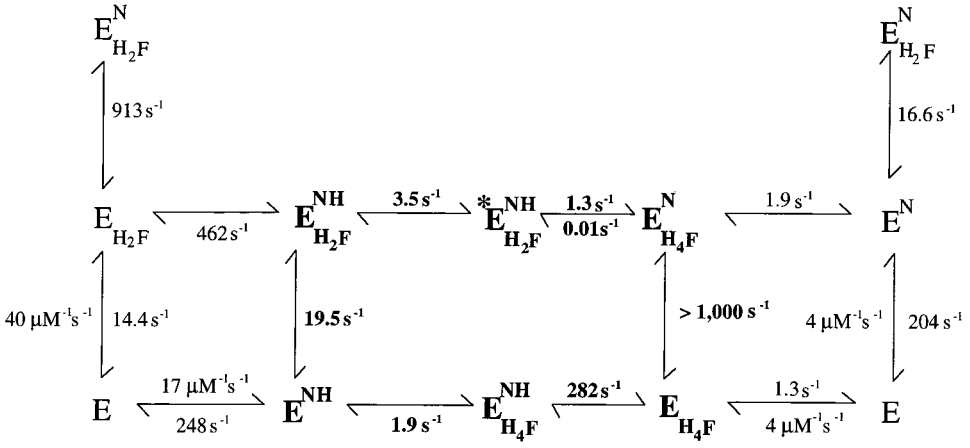

[a] N, $NADP^+$; NH, NADPH.

Scheme 3: Kinetic Scheme for Wild-Type Dihydrofolate Reductase at 25 °C in MTEN Buffer at pH 7.0

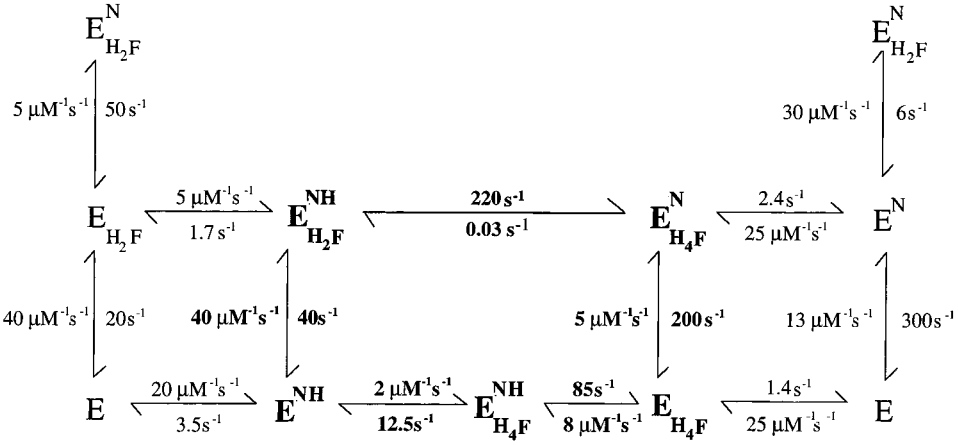

changing the order in which the reaction is initiated. Structural studies of G121V may help to clarify this issue.

Wild-type DHFR exists in two conformational states: E_1 and E_2 with a K_{eq} of 1 for the two forms. While E_1 binds NADPH with a K_d of 0.3−0.4 μM (Table 1 and (*26*)), E_2 binds NADPH with a K_d of 14 μM (*26*). Therefore, it is possible that the absence of a rapid fluorescence change upon binding of NADPH may indicate that the Val-121 mutation has shifted the equilibrium between E_1 and E_2 in favor of E_2. Consistent with this possibility was the finding that the K_d for NADPH binding to Val-121 DHFR is identical to that measured by Adams *et al.* (*26*) for the E_2 conformer of wild-type DHFR. Alternatively, the absence of a rapid NADPH-dependent fluorescence change may indicate that the rate of positioning of the reduced nicotinamide moiety of NADPH in the enzyme for optimal energy transfer is slower than binding. This possibility is discussed further below.

Measurement of the various equilibrium binding constants (Table 1), dissociation rate constants (Table 2), and forward (Figures 3−6) and reverse rate constants for hydride transfer permitted the construction of a kinetic scheme for Val-121 DHFR at pH 7.0 (Scheme 2). Only the association rate constants for H_2F and H_4F were measured directly. Information on the dissociation rate constants of ligands from the reactive ternary complex was approximated by using DNADPH in place of NADPH. In addition to the increased rates of dissociation for NADPH from the binary and various ternary complexes and for $NADP^+$ from the ternary product complex, there are two very striking differences between the partial kinetic scheme describing the forward reaction for Val-121 DHFR and that elaborated by Fierke *et al.* for the wild-type enzyme (Scheme 3).

First, the rate of hydride transfer was reduced by approximately 200-fold relative to that of wild-type DHFR at pH 7.0; thus, hydride transfer is partially rate limiting in both the pre- and steady state. In contrast, steady-state turnover by wild-type DHFR is limited by H_4F release (*4*). The fact that the rate of hydride transfer was contributing to the observed kinetics was clearly supported by the existence of a primary isotope effect of 2.4 and 2.1 on the pre-steady-state and steady-state rates, respectively (Figures 3 and 4). Such a pronounced effect on hydride transfer under saturating conditions of substrate and cofactor by a single amino acid substitution 19 Å from the active site was not expected.

Second, a conformational change was observed that preceded the chemical step. This conformational change was manifested in an apparent burst which occurred at a rate of 3.5 s^{-1} when stopped-flow fluorescence energy transfer was used to monitor hydride transfer (Figure 4). As there was no isotope effect on the burst rate (Figure 4), it was clear that the observed fluorescence change could not be related to hydride transfer *per se*. The rate measured was, in fact, first order, consistent with this transient arising from a conformational change (Figure 5). Finally, when stopped-

flow absorbance was used to monitor NADPH consumption, a 50 ms lag was observed which was very good evidence for the existence of a conformational change step preceding chemistry in the kinetic scheme for Val-121 DHFR (Figure 6).

Based on the experimental design, the observed conformational change must be associated with a rearrangement of the reduced nicotinamide moiety of NADPH into an environment or conformation for efficient energy transfer, presumably the enzyme active site. The final position of the nicotinamide moiety in the catalytic site of the mutant enzyme is probably similar to wild-type DHFR since the extent of quenching of intrinsic enzyme fluorescence (80%) by this molecule was the same for both enzymes (Figure 2 and data not shown). Such a rearrangement of the nicotinamide ring has been shown by Eklund and co-workers to be required for hydride transfer catalyzed by the NADH-dependent horse liver alcohol dehydrogenase (*27*). In addition, having a conformational change which precedes chemistry and occurs on the same time scale explains the inability to observe a full isotope effect of 2.8 on the measured rate of hydride transfer for Val-121 DHFR (*4*). Whether the conformational change described here is related to the movement of the βF−βG loop observed crystallographically is not clear.

While a conformational change preceding the chemical step has been noted for the mouse and human DHFRs (*28*), no evidence exists for such a step in the mechanism of *E. coli* DHFR. If the kinetic scheme for wild-type DHFR were to include a conformational change prior to the chemical step, then a rate constant greater than 2000 s^{-1} would be a reasonable estimate because a full isotope effect of 2.8 is observed on the rate of hydride transfer (*4*). Such a fast rate would not be observed by stopped-flow fluorescence because the dead time of the instrument is 2 ms. The ability to place a conformational change step in the mechanism of *E. coli* DHFR-catalyzed hydride transfer would reconcile many discrepancies between the kinetic scheme for this enzyme and that described for the vertebrate enzymes. Moreover, the existence of this step in the mechanism of the wild-type enzyme would suggest that the overall mechanism used by Val-121 DHFR is conserved and only the rates of these steps are affected. Additional studies are required to clarify this issue.

All substitutions and insertions at position 121 decrease the rate of hydride transfer (Table 3). Furthermore, with the exception of substitutions of alanine and serine and insertion of glycine, all mutant DHFRs described herein caused the appearance of a conformational change preceding hydride transfer (Table 3). The ability of alanine and serine to be accommodated, for the most part, at this position is consistent with these residues being located at the structurally homologous position in DHFRs of vertebrate origin (*29*). These data, however, illustrate the critical nature of this residue for the catalytic process. In fact, these data suggest that this residue, quite remote from the active site, is as critical as those comprising the active site. This was not expected. Such a strong influence of remote sites on catalysis presents yet another challenge for the design of enzymes *de novo*.

Taken together, the data presented herein have shown that by changing a single amino acid which exhibits unique dynamic properties and is located 19 Å from the catalytic center, a mutant enzyme can be produced which has a significant reduction in the rate of conformational change (500-fold), the rate of hydride transfer (200-fold), and binding to NADPH (40-fold). While the molecular basis for the observed changes is not known, two scenarios can be envisaged. First, changing glycine-121 may produce a structural perturbation in the βF−βG loop due to the inability of a side chain to interact properly with loop I, thereby altering the interaction of loop I with elements of the active site required for proper positioning of NADPH and hydride transfer (Figure 1). It is also possible that changing glycine-121 alters the dynamic features of this residue and/or the βF−βG loop. If catalysis requires the sampling of a population of active site conformations and only a subset of these conformations are catalytically competent, then by changing the dynamics of this process conformational changes and chemistry would be necessarily affected. Because these two possibilities are not mutually exclusive, structural and dynamic studies of the mutants described herein will be necessary to clarify this issue.

ACKNOWLEDGMENT

C.E.C. is grateful to members of the Benkovic laboratory for very helpful discussions during the completion of these studies, to Dr. William Cannon for preparation of Figure 1, and to J. Arnold for assistance in preparation of the manuscript.

REFERENCES

1. Sawaya, M. R., and Kraut, J. (1997) *Biochemistry 36*, 586−603.
2. Falzone, C. J., Wright, P. E., and Benkovic, S. J. (1994) *Biochemistry 33*, 439−442.
3. Epstein, D. M., Benkovic, S. J., and Wright, P. E. (1995) *Biochemistry 34*, 11037−11048.
4. Fierke, C. A., Johnson, K. A., and Benkovic, S. J. (1987) *Biochemistry 26*, 4085−4092.
5. McCammon, J. A., and Harvey, S. C. (1987) *Dynamics of Proteins and Nucleic Acids*, Cambridge University Press, Cambridge, U.K.
6. Creighton, T. E. (1993) *Proteins: Structure and Molecular Properties*, W. H. Freeman, New York.
7. Farnum, M. F., Magde, D., Howell, E. E., Hirai, J. T., Warren, M. S., Grimsley, J. K., and Kraut, J. (1991) *Biochemistry 30*, 11567−11579.
8. Li, L., Falzone, C. J., Wright, P. E., and Benkovic, S. J. (1992) *Biochemistry 31*, 7826−7833.
9. Bystroff, C., and Kraut, J. (1991) *Biochemistry 30*, 2227−2239.
10. Kraulis, P. J. (1991) *J. Appl. Crystallogr. 24*, 946−950.
11. Gekko, K., Kunori, Y., Takeuchi, H., Uhihara, S., and Kodama, M. (1994) *J. Biochem. 116*, 34−41.
12. Blakley, R. L. (1960) *Nature (London) 188*, 231−232.
13. Mathews, C. K., and Huennekens, F. M. (1960) *J. Biol. Chem. 235*, 3304−3308.
14. Curthoys, H. P., Scott, J. M., and Rabinowitz, J. C. (1972) *J. Biol. Chem. 247*, 1959−1964.
15. Jeong, S. S., and Gready, J. E. (1994) *Anal. Biochem. 221*, 273−277.
16. Kallen, J. R., and Jenks, W. P. (1968) *J. Biol. Chem. 241*, 5845−5850.
17. Dawson, R. M. C., Elliott, D. C., Elliott, W. H., and Jones, K. M. (1969) *Data for Biochemical Research*, p 199, Oxford University Press, Oxford, U.K.
18. Seeger, D. R., Cosulich, D. B., Smith, J. M., and Hultquist, M. E. (1949) *J. Am. Chem. Soc. 71*, 1753−1758.
19. P-L Biochemicals (1961) *Circular OR-18*, P-L Biochemicals, Milwaukee, WI.

20. McPherson, M. J., Quirke, P., and Taylor, G. R. (1991) *PCR: A Practical Approach*, Oxford University Press, Oxford, U.K.
21. Sambrook, J., Fritsch, E. F., and Maniatis, T. (1989) *Molecular Cloning: A Laboratory Manual*, Cold Spring Harbor Laboratory Press, Cold Spring Harbor, NY.
22. Aiyar, A., Xiang, Y., and Leis, J. (1996) *Methods Mol. Biol. 57*, 177−191.
23. Lakowicz, J. R. (1983) *Principles of Fluorescence Spectroscopy*, Plenum Press, New York.
24. Cannon, W. R., Garrison, B. J., and Benkovic, S. J. (1997*) J. Am. Chem. Soc. 119*, 2386−2395.
25. Cannon, W. R., Singleton, S. F., and Benkovic, S. J. (1996) *Nat. Struct. Biol. 3*, 821−833.
26. Adams, J. A., Fierke, C. A., and Benkovic, S. J. (1991) *Biochemistry 30*, 11046−11054.
27. Eklund, H., Samama, J. P., and Jones, T. A. (1984) *Biochemistry 23*, 5982−5996.
28. Beard, W. A., Appleman, J. R., Delcamp, T. J., Freisheim, J. H., and Blakley, R. L. (1989) *J. Biol. Chem. 264*, 9391−9399.
29. Oefner, C., D'Arcy, A., and Winkler, F. K. (1988) *Eur. J. Biochem. 174*, 377−385.

BI9716231